Journal of Physics B: Atomic, Molecular and Optical Physics

PAPER • **OPEN ACCESS**

Electron ionisation of cyanoacetylene: ionisation cross sections and dication formation

To cite this article: Lilian K Ellis-Gibbings *et al* 2022 *J. Phys. B: At. Mol. Opt. Phys.* **55** 124001

OPEN ACCESS
IOP Publishing
Journal of Physics B: Atomic, Molecular and Optical Physics
J. Phys. B: At. Mol. Opt. Phys. **55** (2022) 124001 (14pp)
https://doi.org/10.1088/1361-6455/ac6781

Electron ionisation of cyanoacetylene: ionisation cross sections and dication formation

Lilian K Ellis-Gibbings[1,*], Bridgette Cooper[2], Jonathan Tennyson[2] and Stephen D Price[1]

[1] Department of Chemistry, University College London, London WC1H 0AJ, United Kingdom
[2] Department of Physics and Astronomy, University College London, London WC1E 6BT, United Kingdom

E-mail: lily.ellis-gibbings@npl.co.uk

Received 31 January 2022, revised 30 March 2022
Accepted for publication 13 April 2022
Published 24 May 2022

Abstract

Cyanoacetylene (HC_3N) is an important trace species in the atmosphere of Titan. We report, for the first time, absolute partial electron ionisation cross sections and absolute precursor-specific partial electron ionisation cross sections for cyanoacetylene, following an experimental and computational investigation. Our methodology involves using 2D ion–ion coincidence mass spectrometry to generate relative cross sections, over the electron energy range 50–200 eV. These relative values are then normalised to an absolute scale, using a binary encounter-Bethe (BEB) calculation of the total ionisation cross section. The BEB calculation agrees well with previous determinations in the literature. The mass spectrometric observations of HC_2N^+ and HCN^+, ions with a connectivity markedly different to that of the neutral molecule, point towards a rich cationic energy landscape possessing several local minima. Indeed, $[HC_3N]^{2+}$ minima involving a variety of cyclic configurations are revealed by a preliminary computational investigation, along with two minima with linear and bent geometries involving H atom migration ($CCCNH^{2+}$). Determination of the energy of a transition state between these local minima indicates that the dication is able to explore the majority of this rich conformational landscape at our experimental energies. This investigation of the energetics also determines an adiabatic double ionisation energy of 30.3 eV for the lowest lying singlet state of $HCCCN^{2+}$, and 30.1 eV for the lowest-lying triplet state. The bulk of the cation pairs detected in the coincidence experiment appear to originate from markedly excited dication states, not the ground state. We observe 5 two-body dissociations of $HCCCN^{2+}$, and subsequent decay of one of the ions generated in such two-body processes accounts for the majority of three-body dissociations we observe.

Keywords: electron ionisation, ionisation, cross sections, cyanoacetylene, HCCCN, HC_3N, energetics

Supplementary material for this article is available online

(Some figures may appear in colour only in the online journal)

* Author to whom any correspondence should be addressed.

1. Introduction

Cyanoacetylene (HC_3N) is the smallest cyanopolyyne, identified spectroscopically in interstellar clouds in 1971 [1] via the hyperfine splitting of the $J = 0$–1 transition, and later via the v_6 and v_5 fundamental vibration-rotation bands at 500 and 663 cm^{-1} [2], respectively. Cyanoacetylene has also been detected in protoplanetary disks beyond the water freezing snow line [3], in comets [4], and in the atmosphere of Titan by Voyager 1^2 and Cassini [5]. It has been proposed that formation of cyanoacetylene in these environments is via the reaction of CN with acetylenes [2, 6, 7], or CN with C_2H radicals [7]. Other potential formation pathways include dissociative recombination of cations [8] and associative detachment of anions [9]. Cyanoacetylene is a potential precursor to larger nitriles [10], a component of prebiotic synthesis of various ribonucleotides [11], and is known to undergo photolysis in Titan's atmosphere [12]. The presence of cyanoacetylene in these energetic environments necessarily results in its ionisation. Hence, characterization of the ionisation of cyanoacetylene is required for modelling both its abundance and its contribution to the chemistry of these regions. In fact, such studies are already underway, with theoretical and experimental investigations of cyanoacetylene's chemical interactions [13].

This paper reports an investigation of the electron ionisation of cyanoacetylene. Pertinent previous work includes experimental, and theoretical, determinations of various electron collision cross sections [14, 15], ground and excited state energy and geometry determinations [14, 16–19], the appearance energies and enthalpies of formation of the products of electron ionisation [16, 20], neutral reactions [6], cation reactions [8, 13], anion reactions [9] and photon-initiated processes [12, 17, 21]. Despite the breadth of these studies, we can find no reports of partial electron ionisation cross sections of cyanoacetylene in the literature, nor any detailed studies of the cyanoacetylene dication. To address this shortcoming, this article reports values of the partial ionisation cross sections (PICSs) and precursor-specific partial ionisation cross sections (PS-PICSs, definition below) for electron ionisation of cyanoacetylene over the energy range 50–200 eV. The PS-PICS quantify not only the cross section for formation of an individual fragment ion, but also quantify the contribution to that ion yield from each level of ionisation of the parent (single, double, triple, …). Relative PICS and PS-PICS are first determined from an ion–ion coincidence experiment [22]. The binary encounter Bethe (BEB) model is then employed to calculate the total ionisation cross section at each electron energy investigated, and these total ionisation cross sections are used to place the relative experimental values on an absolute scale, as described in detail in previous work [23]. A complementary computational study of the dication states reveals a rich geometric landscape allowing a rationalization of the unimolecular dissociation of HC_3N^{2+} we observe in our experiments.

2. Methodology

2.1. Coincidence mass spectrometry

2.1.1. Experimental operation. The coincidence mass spectrometer employed in this work has been described in detail before in the literature [24] and, hence, is only briefly described here. The high-vacuum experiment involves a beam of electron pulses which cross an effusive gas jet of the target molecule in the centre of the pulsed source field of a two-field time of flight mass-spectrometer (TOF-MS). The TOF-MS utilises a microchannel plate (MCP) detector and coincidence counting electronics involving a programmable time-to-digital converter for data collection. In these experiments, the pressure of the target molecule (cyanoacetylene), measured by an ion gauge remote from the collision region, is kept close to 10^{-6} Torr. Experiments have shown this pressure regime ensures single collision conditions, and, on average, much less than one ionisation event per electron pulse. The ionising electron pulses, produced from a tungsten filament, are 30 ns in duration with a repetition rate of 50 kHz. The energy spread of the electron beam is approximately 0.5 eV, and the nominal electron kinetic energies employed in our series of experiments lie between 50–200 eV. The electrons and the target gas jet cross perpendicular to both each other and to the principal axis of the TOF-MS. Following the ionising electron pulse, the repeller plate of the extraction region is pulsed from 0 to +400 V to extract cationic products towards the detector. The TOF-MS is of a standard Wiley–McLaren design [25] and the extraction is efficient, collecting ions with up to 15.5 eV of kinetic energy transverse to the TOF-MS axis [26]. The ion signals from the MCP detector are recorded as arrival times by a time-to-digital converter, which records multiple stop signals for a single ionising electron pulse. Up to three ions are detected in coincidence per cycle, as a single ion, pair of ions, or triple of ions. These signals are accumulated in a memory module and subsequently transferred to the analysis PC. The term 'true pair' refers to two ions, detected in coincidence, that arise from the same ionising event, usually dissociative double ionisation. Similarly, 'true triples' refers to three ions, detected in coincidence, that arise from the same event, usually dissociative triple ionisation.

Calibration of the time-of-flight mass scale is performed by recording mass spectra of Ar. This preliminary investigation, involving the measurement of the ratio of Ar^+ to Ar^{2+}, also confirms there is no intrinsic mass discrimination in our experiments [27]. Similarly, a determination of the ion detection efficiency f of the apparatus is achieved by recording the spectrum of CF_4, a molecule for which the cross sections for generating the singles and pairs are well established [28, 29]. The overall ion detection efficiency was determined to be 0.29, in good accord with previous determinations for our apparatus. Coincidence datasets are recorded at each ionising electron energy of interest, the electron energy of successive measurements being varied in a non-systematic manner to avoid any hysteresis. Recording a single dataset involves a continuous

experiment, lasting 6–8 h, which typically collects over 6 million singles and 170 thousand pairs.

Cyanoacetylene is a colourless liquid at room temperature with a melting point near 5 °C [30] and a boiling point at 41.8 °C [31]. Cyanoacetylene was synthesised in-house following a standard methodology [11]. A detailed description of the synthesis is available in the supplementary information (SI section S.2 partial ionisation cross sections) (https://stacks.iop.org/JPB/55/124001/mmedia). The cyanoacetylene sample was transferred to, and kept in, a glass cold finger under vacuum, on the inlet gas-line of the TOF-MS. The sample was maintained as a solid during experiments, held at 0 °C using an ice-water bath, to limit reactivity and degradation. At this temperature, the vapour pressure of the solid was low but sufficient for admission to the TOF-MS. Unfortunately, the low sample vapour pressure resulted in a larger fluctuation than normal in the pressure of the target molecule in the mass spectrometer. These fluctuations result in slightly larger uncertainties in the cross sections of the minor product ions than a typical coincidence dataset. Using the above methodology, the pressure of the cyanoacetylene in the mass spectrometer's inlet system was also markedly lower than we would usually employ. Under these conditions, the relative partial pressure of the background gas (principally air and water) in the apparatus is larger than in a typical set of experiments. Thus, the mass spectra show larger 'background' peaks from air (O_2, CO_2, N_2, H_2O) than in our typical spectra. These disadvantages of operating at a low sample pressure are however far outweighed by the advantage of maintaining a stable un-degraded sample of cyanoacetylene. The contaminant peaks, which usually range in intensity from 0%–5% of the parent cation signals, are mostly well-separated from the signals resulting from cyanoacetylene and do not interfere with our analysis. Where any contaminant peaks do interfere with those of interest, as for example with N^+, we remove the contaminant component in a method described below using the known relative PICS for the contaminant species. Aside from these air-related peaks, the TOF-MS showed the HC_3N sample was remarkably pure (>99%) after several freeze-pump-thaw cycles. A highly reactive molecule, HC_3N oligomerises rapidly [21] in the presence of water and, over time (weeks), an oily black residue did form on the inner surface of the glass cold finger despite the low temperature. As the mass spectrum of the sample remained unchanged throughout, this solid product clearly has a very low vapour pressure, consistent with its identification as an oligomer.

2.1.2. Processing of coincidence data. When a single ion is detected by the TOF-MS following a pulse of the repeller plate, we term the event a 'single' and the flight time is added to a list of such events. From this data the 'singles' mass spectrum is produced as a histogram, of ion counts against time of flight. From the singles mass spectrum the intensity $I[X^+]$ of each ion X^+ is determined by summing the counts in each peak and subtracting the appropriate non-zero background. For pair events, when two ions are detected in coincidence, the flight times of both ions are recorded.

Pair events are displayed in a two-dimensional 'pairs spectrum': a two-dimensional histogram of counts (z), t_1 (flight time of faster ion, y) vs t_2 (flight time of slower ion, x). Individual dication (or trication) charge-separating dissociation reactions appear as distinct lozenge-shaped peaks in such a pairs spectrum. Summing the counts in the various peaks involving a given ion, after removing any false coincidences (see below), allows us to evaluate the detected intensity for a given ion (e.g. CH^+) in the pairs spectrum, $P[X^+]$. A distinction is made between the intensity of ions in pairs involving a pair of monocations which we designate $P_2[X^+]$, and the intensity of a given ion in pairs which must result from triple ionisation (the pair involves a monocation and a dication), which we designate $P_3[X^+]$ and $P_3[X^{2+}]$, for the cation and dication respectively.

The flight times involved in ion triples are again stored in an event list. To analyse these events we generate a two-dimensional histogram for the values of t_2 and t_3 that are associated with a particular range for t_1, that range of t_1 corresponds to a given product ion (e.g. H^+). Such a plot identifies the two ions in any triple which are coincident with the specified ion (H^+ in the above example). Careful choice of different specified ions, and the generation of a number of these triples spectra, allows all of the triples to be analysed. The intensities of all the triples peaks are again determined by summing the counts and subtracting an estimate of the contribution of false coincidences. Such a procedure allows us to derive the intensity of a given ion in the triples spectrum: $T_3[X^+]$. The number of 'triples' detected is significantly lower than the number of 'pairs' in the electron energy regime we investigate, and the number of real quadruple arrivals is negligible. Therefore, as in our previous investigations with this instrument [23, 24, 32, 33], we do not collect or process any quadruple arrival events and neglect the very minor contribution of quadruple ionisation to our data set.

As noted above, the intensities of all the peaks in the singles spectrum are corrected for the non-zero background in the singles spectrum [34]. Additionally, the peaks at m/z values of 1, 6, 7, 12 and 14 contain contributions from the background H_2O, CO_2 and N_2 present in the system. Such contributions can be estimated and subtracted using the known PICSs [33, 35–37] for these contaminants and the intensity of a mass peak unambiguously assignable to the contaminant. In general, the contribution of these background gases to a mass peak from cyanoacetylene is quite low, less than 5% of the total intensity of the peak in question. However, the N^+ peak was found in some spectra to have up to a 50% contribution from ionisation of N_2. All other peaks originating from background gases are well separated from peaks of interest, and do not interfere with the analysis of the pairs and triples spectra.

As noted above we subtract an estimate of the number of false coincidences from each coincidence peak in the pairs and triples spectrum. False coincidences [33] are events involving the detection of two or three ions that do not result from the same ionisation event. The contribution of false coincidences to each pairs and triples spectrum is minimised experimentally by operating at low ion count rates, but a small contribution

from such events is still present in the data. The contribution of false coincidences to the intensity of the coincidence peaks of interest is quantified and subtracted using a well-established ion-autocorrelation procedure [34]. Additionally, the ion detection system has a dead-time of 32 ns between detectable ion hits. This dead-time restricts the detection of ion pairs with the same m/z ratio. These deadtime losses can easily be estimated by generating a histogram, of intensity vs $t_2 - t_1$ for a given reaction. In such a time-of-flight difference ($t_2 - t_1$) spectrum, the coincidence signals have a characteristic square shape. Signal losses due to the deadtime are readily apparent in such time-of-flight difference spectra and can be readily assessed by extrapolating the square peak back to $t_2 - t_1 = 0$ [34]. Such time of flight difference spectra also reveal those ion pairs where some signal is lost due to high transverse kinetic energies of the ions [33]. Such losses of high-energy ions result in a hollowing of the normally square signals in the difference spectra. In the case of cyanoacetylene this final correction was explored, but not required for any dissociation process. We are unable to correct for the losses of energetic (>15.5 eV) fragment ions from single ionisation, but we expect such ions to be a very minor component of the ion yield.

Our data analysis methodology to generate the PICS and the PS-PICS has been described in detail before [24, 34, 38] and will be only briefly discussed here. Relative PICS ($\sigma_r[X^+]$ and $\sigma_r[X^{2+}]$) are generated from the experimental data, for each ion detected, in the following way (using a singly charged cation as an example):

$$\sigma_r[X^+] = \frac{\sigma[X^+]}{\sigma[HC_3N^+]} \tag{1}$$

$$\sigma_r[X^+] = \sigma_1[X^+] + \sigma_2[X^+] + \sigma_3[X^+] \tag{2}$$

$$\sigma_n[X^+] = kN_n[X^+] \tag{3}$$

$$\sigma_r[X^+] = \frac{N_1[X^+] + N_2[X^+] + N_3[X^+]}{N_1[HC_3N^+]} = \frac{I_1[X^+] + P_2[X^+] + P_3[X^+] + T_3[X^+]}{I[HC_3N^+]}. \tag{4}$$

In equations (1)–(4), $\sigma_n[X^+]$ is the precursor-specific relative PICS for the formation of X^+ in an ionisation event involving the loss of n electrons from HCCCN, where $n = 1$, 2, or 3. $N_n[X^+]$ is the number of fragment ions X^+ formed by ionisation events involving the loss of n electrons, and k is a proportionality constant dependent on the individual experiment (pressure, electron flux), this constant is eliminated in deriving the relative cross section in equation (4).

To determine the PS-PICS, the detection efficiency f of the apparatus is combined with the corrected counts from the experimental data. To determine the PS-PICS for X^+ and X^{2+} representative equations are as follows:

$$\sigma_1[X^+] = \frac{I[X^+] - \left(\frac{1-f}{f}\right)\{P_2[X^+] + P_3[X^+]\} + \left(\frac{1-f}{f}\right)^2 T_3[X^+]}{I[HC_3N^+]} \tag{5}$$

$$\sigma_2[X^+] = \frac{\left(\frac{1}{f}\right)P_2[X^+] - 2\left(\frac{1-f}{f^2}\right)T_3[X^+]}{I[HC_3N^+]} \tag{6}$$

$$\sigma_3[X^+] = \frac{\left(\frac{1}{f}\right)P_3[X^+] - \left(\frac{1}{f^2}\right)T_3[X^+]}{I[HC_3N^+]} \tag{7}$$

$$\sigma_2[X^{2+}] = \frac{I[X^{2+}] - \left(\frac{1-f}{f}\right)P_3[X^{2+}]}{I[HC_3N^+]} \tag{8}$$

$$\sigma_3[X^{2+}] = \frac{\left(\frac{1}{f}\right)P_3[X^{2+}]}{I[HC_3N^+]}. \tag{9}$$

Using equations (4)–(9), the relative PICS and PS-PICS can be determined for all ions we detect following the ionisation of cyanoacetylene [39]. For both the PICS and PS-PICS, the experimental uncertainty associated with each value is taken as two standard deviations from the mean of the values derived from the three datasets for each energy. Relative uncertainties are relatively high, unsurprisingly, at PICS values close to our experimental detection limit, that is for the low abundance ions such as N^{2+} and C_2NH^{2+} at electron energies of 50 eV and 75 eV. To generate absolute values from the relative cross sections, we normalise to a BEB calculation of the total ionisation cross section over the energy range of interest, as described in our recent publication [23].

Information on the energetics and dynamics accompanying the dissociation of double-ionised cyanoacetylene can be extracted from the pairs spectra [34, 40–42]. This analysis is performed on spectra recorded at an ionising energy of 75 eV, the lowest energy with sufficient count-rates for meaningful analysis of the shapes of the coincidence signals. In brief, the analysis involves extracting the gradient and $t_2 - t_1$ spectrum of each peak in the pair spectrum, each peak corresponding to a given dissociation reaction [43]. The gradient, which reveals the correlation between the momenta of the fragment ions, can be compared with that expected for a variety of dissociation mechanisms [41]. These peak gradients are extracted from the pairs spectra with a weighted least squares analysis [40, 41]. The kinetic energy release (KER) of an individual dissociation reaction is extracted by fitting a Monte Carlo simulation of the dissociation process to the experimental $t_2 - t_1$ spectrum extracted from a given dissociation channel [23]. Such Monte Carlo simulations, which incorporate the full range of experimental conditions, have been shown to extract KERs in excellent agreement with those reported in the literature [23]. The appropriate model parameters characterizing the KER (magnitude, distribution) are refined until a good fit is achieved with the experimental $t_2 - t_1$ data. The KERs produced have a range of satisfactory fit to the experimental data of approximately 0.5 eV, and this value is taken as the uncertainty of the derived KER. Previous work has shown that our experimental arrangement efficiently detects the light H^+ fragments, but an asymmetry of the coincidence peaks involving H^+ arises from penetration into the source region of the electric field from the drift tube [38]. Due to this asymmetry it is not instructive to interpret the shapes of the coincidence peaks involving H^+ in terms of the dynamics of the dissociation of the dication.

Once a value for the KER of a given dissociation channel has been determined, the energy of the dication precursor state of cyanoacetylene, $E[HC_3N^{2+}]$, associated with the formation of that ion pair, can be evaluated by adding the value of the KER to the asymptotic energy of the products (E_{frag}) obtained from thermodynamic data:

$$E\left[HC_3N^{2+}\right] = \mathrm{KER} + E_{\mathrm{frag}}. \tag{10}$$

Such precursor state energies have proved valuable in providing a coarse probe of the energies of the low-lying electronic states of dications [38].

2.2. Computational investigations

2.2.1. Electronic structure calculations. Electronic structure calculations using Gaussian16 (Rev. A03) [44] have been used to help interpret our experimental findings. Equilibrium geometries, and adiabatic and vertical ionisation energies, where appropriate, have been determined for the linear $HCCCN^{2+}$ structure. Similar determinations have also been made for several other cyclic and bent local minima that were located on the $[HCCCN]^{2+}$ energy landscape for both the singlet and triplet multiplicities. Stationary points were determined with a B3LYP methodology, employing a cc-pVTZ basis set. This density functional theory (DFT) approach, given our computational budget, gave a much better agreement with the accepted literature geometries and energetics of neutral [18] and singly-ionised [19] HCCCN than the MP2 methodology we have employed before. We presume that the DFT approach is superior here due to the significant multi-reference character of some of the states [19]. All the minima we located were verified by vibrational frequency analysis which also determined the associated zero point energy. The energetics of the stationary points were determined using single-point CCSD(T) calculations using the same basis set. As described in more detail below, we also searched for transition states linking the local dicationic minima.

2.2.2. Total ionisation cross section calculation (BEB). As discussed above, we use calculated values of the total ionisation cross section to place the relative cross sections we derive from our experimental data onto an absolute scale. This procedure has been discussed in detail in the recent literature [23]. For the calculation of the total ionisation cross section we use a binary-encounter Bethe (BEB) methodology [45]. This semi-empirical approach requires only the occupation, binding and average kinetic energies of the electrons in the occupied orbitals of the target molecule. The method, originally developed by Kim and Rudd [45], is used as implemented in the Quantemol electron collisions expert system [46, 47]. The present all-electron BEB calculations were performed using Hartree–Fock target wavefunctions and the cc-pVTZ basis set, with the linear HC_3N geometry optimised at cc-pVDZ. This neutral geometry is again in good agreement with that in the literature [18]. In previous work [23] the uncertainty assigned to the cross section derived from the BEB calculation was better than 5% of the calculated value across the ionising energy range. Thus, in this work, to estimate the final uncertainty in our PICS and PS-PICs we combine a 5% uncertainty in the calculated total ionisation cross section with the determined experimental uncertainty in the relative cross sections. As a comparison, we note that in absolute experimental me asurements, such as those by Stebbings *et al* in a highly sensitive mass analyser, the experimental uncertainties on absolute PICSs are commonly between 5% and 30% [36, 48, 49].

Our algorithm to normalise the relative experimental PICS and PS-PICS to the total ionisation cross section produced by the BEB calculation has been presented in detail before [23]. In brief, we first determine the absolute cross section for formation of the parent monocation (HC_3N^+) from the ratio of the calculated total ionisation cross section and the sum of all the relative PICSs, as a function of electron energy. This absolute cross section for forming the parent ($HCCCN^+$) ion can then be used to transform all the relative partial cross sections to absolute values.

3. Results and discussion

3.1. Coincidence mass spectra and ionisation cross sections

Coincidence mass spectra of cyanoacetylene were recorded at electron ionisation energies between 50 and 200 eV. The singles mass spectrum we record at 75 eV for cyanoacetylene is in good accord with that recorded by Harland at 70 eV [16]. Specifically, as seen in figure 1, the dominant ion generated is the parent cation, HC_3N^+, which, at 200 eV, has a peak height approximately 20 times more intense than the next most intense ions, C_3N^+, C^+ and C_2H^+, while the total number of counts for the HC_3N^+ peak is approximately five times higher than those same comparative ions. As discussed above, due to operating at a low HCCCN pressure to preserve the integrity of the sample, minor contamination by air is visible in the spectrum and clearly shown in figure 1. A small $H_2{}^+$ signal, which is markedly too large to be accounted for by ionisation of water contamination is present. Given the observed quadratic pressure dependence of these small $H_2{}^+$ signals it is reasonable to conclude that this ion is generated by a bimolecular reaction in the ionisation region. Similar bimolecular reactions generating protonated species are well known: for example the production of $NH_4{}^+$ from NH_3 ionisation [50]. As these very weak $H_2{}^+$ signals are bimolecular in origin they are not included in the analysis.

The ions detected and shown in figure 1 form the singles spectra of ionisation of cyanoacetylene, and we conclusively detect the following ionisation products: H^+, C^{2+}, N^{2+}, C^+, CH^+, C_3H^{2+}, N^+, $C_2{}^+$, C_2H^+, HC_3N^{2+}, CN^+, HCN^+, $C_3{}^+$, C_3H^+, C_2N^+, C_2NH^+, C_3N^+, and HC_3N^+. Two ions collected in coincidence form the pairs spectrum of ionisation of cyanoacetylene, shown in figure 2(a), and we conclusively detect the following pairs of ionisation products: $C^+ + C^+$, $C^+ + N^+$, $C^+ + CH^+$, $N^+ + CH^+$, $CN^+ + C_2{}^+$, $CN^+ + C_2H^+$, $H^+ + C^+$, $H^+ + N^+$, $H^+ + C_2{}^+$, $H^+ + CN^+$, $H^+ + C_3{}^+$, $H^+ + C_2N^+$, $H^+ + C_3N^+$, $C_3H^{2+} + N^+$, $C_2{}^+ + C^+$, $C_2H^+ + C^+$, $CN^+ + C^+$, $C_2{}^+ + CH^+$, $CN^+ + CH^+$, $C_2{}^+ + N^+$, $C_2H^+ + N^+$, $C_2N^+ + C^+$, $C_2NH^+ + C^+$, $C_2N^+ + CH^+$,

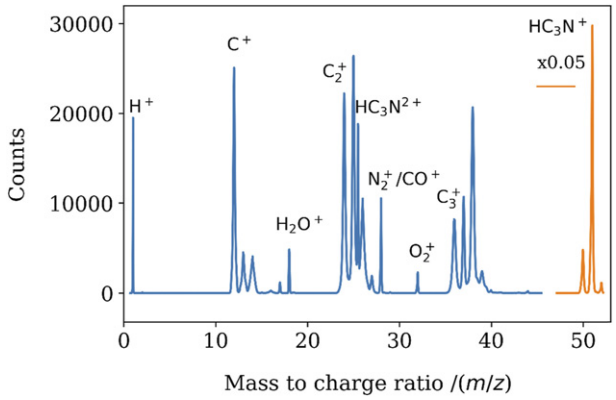

Figure 1. Representative mass spectrum showing the cationic products from the ionisation of HC_3N at 75 eV electron energy. The vertical scale in region 48–52.5 *m*/*z* has been reduced by a factor of 20 to increase visibility of the lower intensity peaks at lower masses. Signals labelled H_2O^+, O_2^+, N_2^+, and CO_2^+ result from traces of background air, a result of the conditions that are required to record stable spectra of the target molecule. Other labels indicate relevant ions from the target molecule. See text for details.

$C_3^+ + N^+$, $C_3H^+ + N^+$, $C^+ + N^{2+}$, $C^+ + C^{2+}$, and $N^+ + C^{2+}$. Three ions collected in coincidence form the triples spectra of ionisation of cyanoacetylene, and we conclusively detect the 13 following triples of ionisation products: $C_2^+ + N^+ + C^+$, $C_2H^+ + N^+ + C^+$, $CH^+ + N^+ + C^+$, $CH^+ + C_2^+ + N^+$, $CH^+ + CN^+ + C^+$, $H^+ + C^+ + C^+$, $H^+ + N^+ + C^+$, $H^+ + C_2^+ + C^+$, $H^+ + C_2^+ + N^+$, $H^+ + CN^+ + C^+$, $H^+ + C_2N^+ + C^+$, $H^+ + C_3^+ + N^+$, $H^+ + CN^+ + C_2^+$.

The total ionisation cross section of cyanoacetylene, calculated using the BEB method and used to convert our relative PICS and PS-PICS to absolute values, is shown alongside the PICS we derive in the supplementary information (S.2 partial ionisation cross sections and table S1). Gilmore and Field [15] published a BEB calculation of the total cross section for electron ionisation of cyanoacetylene, including a comparison to previous literature. Their calculation utilised the restricted Hartree–Fock method and the Gaussian basis set 6-311G(*d*, *p*), whereas our calculation employed a cc-pVTZ basis set for the BEB calculation, and a cc-pVDZ geometry optimisation of the neutral. Satisfyingly, these differences in methodology only result in a maximum difference of 2.5% between the two calculations over the energy range of interest here (50–200 eV). These differences are well within the assigned 5% tolerance of the calculation. Our calculation also compares well with the ionisation cross section calculation performed by Kaur *et al* [14], who used the complex scattering potential-ionisation contribution method.

The absolute PICS we obtain for the formation of the various ionic products we detect following electron ionisation of cyanoacetylene, after scaling the experimental relative cross sections with the BEB calculation, are reported in table S1, and illustrated graphically in figures 3–5 as well as figure S2. Similarly, the resulting absolute PS-PICS are presented in table S2 and figure 6. No reports of previous measurements of these quantities could be found in the literature. Ion appearance energies [16, 20] following ionisation of cyanoacetylene have been reported before, but are at energies below those employed in our study.

As has been observed before for the electron ionisation of small molecules [51], the PICS we report do not vary dramatically over the ionising energy range. Indeed, the maximum value of the electron ionisation cross section is commonly found between 20 and 80 eV for molecules of the size of HC_3N [51]. As our measurements begin at 50 eV, they are above the reported first (11.6 eV) [20] and second (31.52 ± 0.15 eV) [16] ionisation limits of cyanoacetylene. As expected in our data, cross sections for the formation of ions, such as C^+ and H^+; with significant contributions from multiple ionisation, as revealed by the PS-PICS, peak at higher energies than those without such a contribution.

The PICS for formation of the parent ion, HC_3N^+, is more than four times larger than the PICS for forming the most abundant fragment ion, C_3N^+. Electron ionisation of acetylene, by comparison [34], yields a fragment ion, CH_2^+, with a higher PICS than the parent, and the PICS for forming the parent ion from acetonitrile [38] is only twice as large as that for forming CH_2CN^+. The PICS for forming the HC_3N^{2+} parent dication is about three orders of magnitude smaller than HC_3N^+, with the formation of smaller dications even less probable.

Figure 3 shows the PICS for forming product ions containing a CN moiety, as well as the N^+ ion, from ionisation of cyanoacetylene. Such ions are potentially pertinent to the chemical origins of life, as they can contribute to the building of larger molecules such as amino acids and N-heterocycles [10, 11]. Of these ions, the formation of C_3N^+, C_2N^+, CN^+ and N^+ exhibit the higher cross sections, while the cross sections for forming C_2NH^+ and HCN^+ are approximately an order of magnitude lower. The formation of C_2NH^+ and HCN^+ both require rearrangement of the nascent parent ion, formed from the neutral via a vertical ionising transition. Such rearrangements will be discussed below.

Figure 4 shows the PICS for the formation of cations that contain carbon chains following electron ionisation of cyanoacetylene, as well as the values for forming H^+. Such carbon containing species are of intertest as they have the potential to undergo addition reactions, building larger chemical species [52]. Notable in this series are the ions C_3H^+ and C_3^+, which display near identical cross sections. Interestingly, the magnitude of the PICS for C_3^+ and C_3H^+ are markedly lower in comparison to the values for C_3N^+. Additionally, the cross section for forming CH^+ is equally as low as the C_3H^+ and C_3^+ values. Together the low prevalence of these three ions indicates that dissociation of either the NCC ≡ CH bond or the HCCC ≡ N bond are infrequent outcomes of electron ionisation of cyanoacetylene. The low PICS for forming N^+ formation (figure 3) support this conclusion. The significant yield, and shape, of the PICS for forming the C^+ ion is largely due to double ionisation, as is clearly revealed by the PS-PICS (figure 6).

Dications are highly reactive and capable of unusual collision chemistry in, for example, planetary ionospheres such as that of Titan [53, 54]. We observe four dications in the mass spectra of cyanoacetylene: HC_3N^{2+}, C^{2+}, N^{2+} and HC_3^{2+}. Of these ions, the formation of the parent dication HC_3N^{2+} has

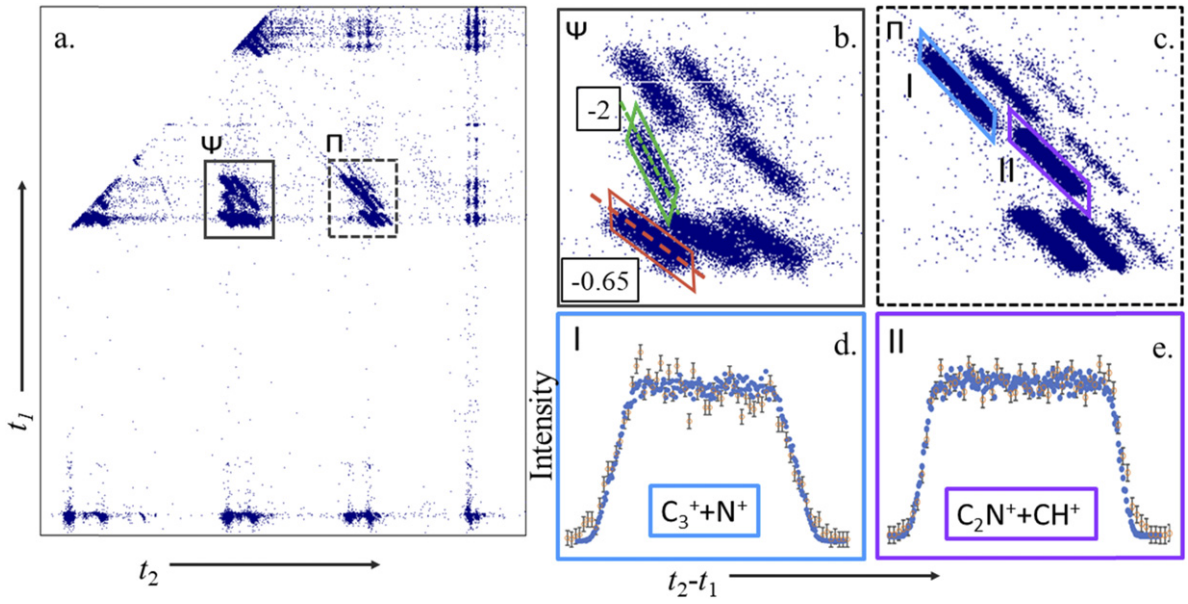

Figure 2. Series of images illustrating aspects of the 2D coincidence mass spectrum. (a) Representative 2D (pairs) coincidence spectrum from the ionisation of HC_3N at 75 eV electron energy. t_1, on the y axis, is the time of flight of the faster ion, with the slower ion TOF on the x axis. (b) Region of the pairs spectrum corresponding to C^+, CH^+ and N^+ on the y axis, and C_2^+, C_2H^+, and CN^+ on the x axis, showing the observable differences in peak slope (labelled) discussed in the text. (c) Region of the pairs spectrum corresponding to C^+, CH^+ and N^+ on the y axis, and C_3^+, C_3H^+, and C_2N^+ on the x axis. (c) also highlights $C_3^+ + N^+$ (blue box, I) and $C_2N^+ + CH^+$ (purple box, II), two peaks that are shown to have two or one kinetic energy releases, respectively. (d) The $t_2 - t_1$ spectrum of the $C_3^+ + N^+$ pair, showing the match between the Monte Carlo simulation (filled blue dots, details in text) and the experimental values (error bars), where the simulation is a fit for two kinetic energy releases of 3.5 eV and 6 eV, respectively. (e) As for (d), for the pair $C_2N^+ + CH^+$, where the simulation is a fit for one kinetic energy release of 3.6 eV. Further details are found in the text.

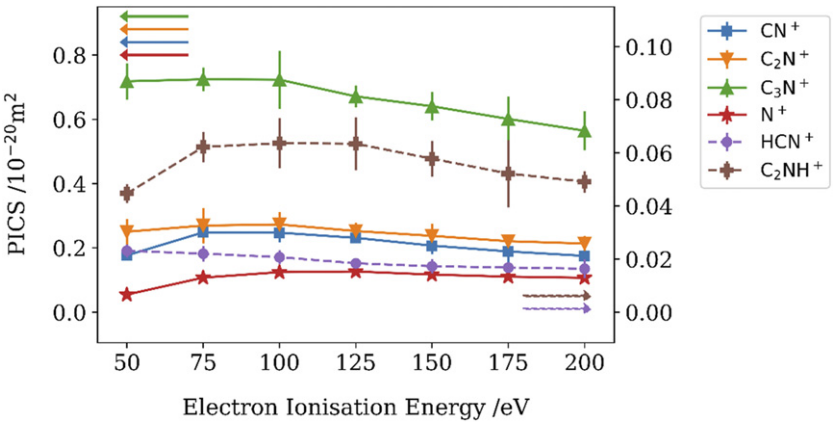

Figure 3. Partial electron ionisation cross sections of HC_3N to form product cations containing the N atom. The dashed lines use the scale of the right axis, as indicated by the arrows.

the largest PICS, with an absolute value comparable with several monocations detected in these experiments. The formation of the other three dications, C^{2+}, N^{2+} and HC_3^{2+}, involves much smaller PICS (figure 5) and these dications are, in fact, the three weakest signals in the cyanoacetylene mass spectra.

The PS-PICS of cyanoacetylene are presented numerically in the supplementary information (table S2) and graphically in figure 6. PS-PICS for HC_3N^+, HCN^+ and HC_3N^{2+} are equal to the PICS for these three ions, as they are formed solely via single ionisation (for HC_3N^+ and HCN^+) or double ionisation (HC_3N^{2+}). The fact that HCN^+ is effectively formed solely by single ionisation is surprising, as the H migration we note in the dication state would appear to allow access to dication geometries which could fragment to this ion. HC_2N^+ is formed via both single and double ionisation, and as we show in the following sections the migration of H to the N position in the dication is certainly possible, which would then provide a pathway to producing HC_2N^+.

The PS-PICS we derive allow an assessment of the contribution of single, double and triple ionisation to the ion yield following an electron collision with HC_3N. At 50 eV, 95% of the total ion yield results from single ionisation, with the remaining 5% from double ionisation. At 100 eV, these proportions are approximately 84% and 16% for single and double

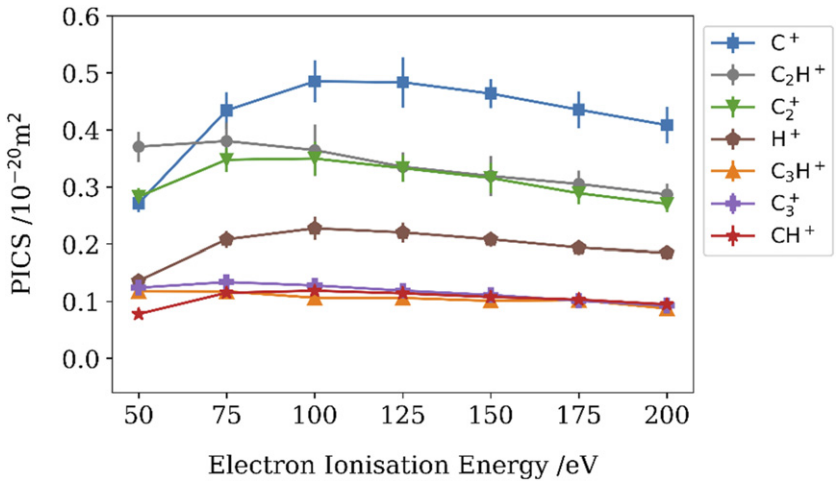

Figure 4. Partial electron ionisation cross sections of HC_3N to form product cations containing C^+, a carbon chain and H^+. See text for details.

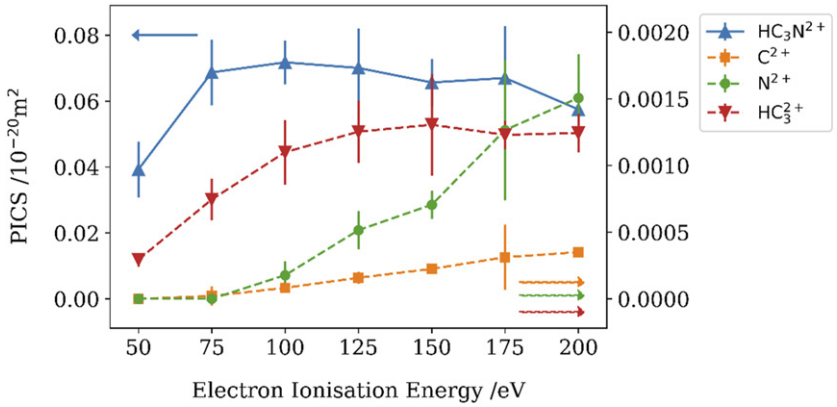

Figure 5. Partial electron ionisation cross sections for the formation of the observed dications following electron ionisation of HC_3N. The dashed lines are aligned with the right axis as indicated by arrows. See text for details.

ionisation, whilst triple ionisation accounts for only 0.5% of all ions produced. At 150 eV and 200 eV single ionisation accounts for close to 83% of ions, with double ionisation contributing just under 17%, and triple ionisation only contributing under 1%. In prior work on PF_3, at 200 eV [23], while the proportion of double ionisation was similar to this case, being around 18%, the proportion of triple ionisation was higher at approx. 3%. This difference indicates that cyanoacetylene has a lower overall cross section for triple ionisation than other molecules studied previously.

The PS-PICS illustrated in figure 6 show similar general trends to these quantities determined for other molecules [34, 38]. For example, the smaller ions, H^+, N^+, CH^+, and CN^+, show the greatest contributions from double and triple ionisation [23]. The two monocations with the largest number of atoms (four), C_3H^+ and C_3N^+, are only formed via single and double ionisation. The thresholds for formation of N^{2+} and C^{2+} via triple ionisation are observed close to electron energies of 125 eV and it appears that significant energy is required to access the dissociation pathways that produce C^{2+} and N^{2+}. In contrast, for most other ions, the PS-PICS for triple ionisation, $\sigma_3[X^+]$ or $\sigma_3[X^{2+}]$ have onsets near 75 eV.

3.2. Dication energetics and geometries

Dications provide access to new ion–neutral chemistry in energetic environments [55], and, as we see above, are generated by the e^- + HCCCN collision system. The monocationic products of the charge-separating dissociations of dications are also implicated in chemical bond formation and unusual chemistry [55]. As described above, we can investigate the energetics of the $HCCCN^{2+}$ dication by extracting the KERs from the coincidence signals of some of the dicationic charge-separating reactions we detect. To help rationalize the energetics derived from these KERs, we have also investigated the geometries and energetics of the $HCCCN^{2+}$ dication computationally. To validate our computational methodology, which has been widely used in other studies of small dications, we have also determined the relative energetics and geometries of neutral and singly ionised cyanoacetylene to compare with established values in the literature [16, 17].

Table 1 shows a subset of the results, those from the most pertinent electronic structure calculations. The full set of geometric and energetic results are detailed in the supplementary information (tables S3–S5). The neutral geometry [18]

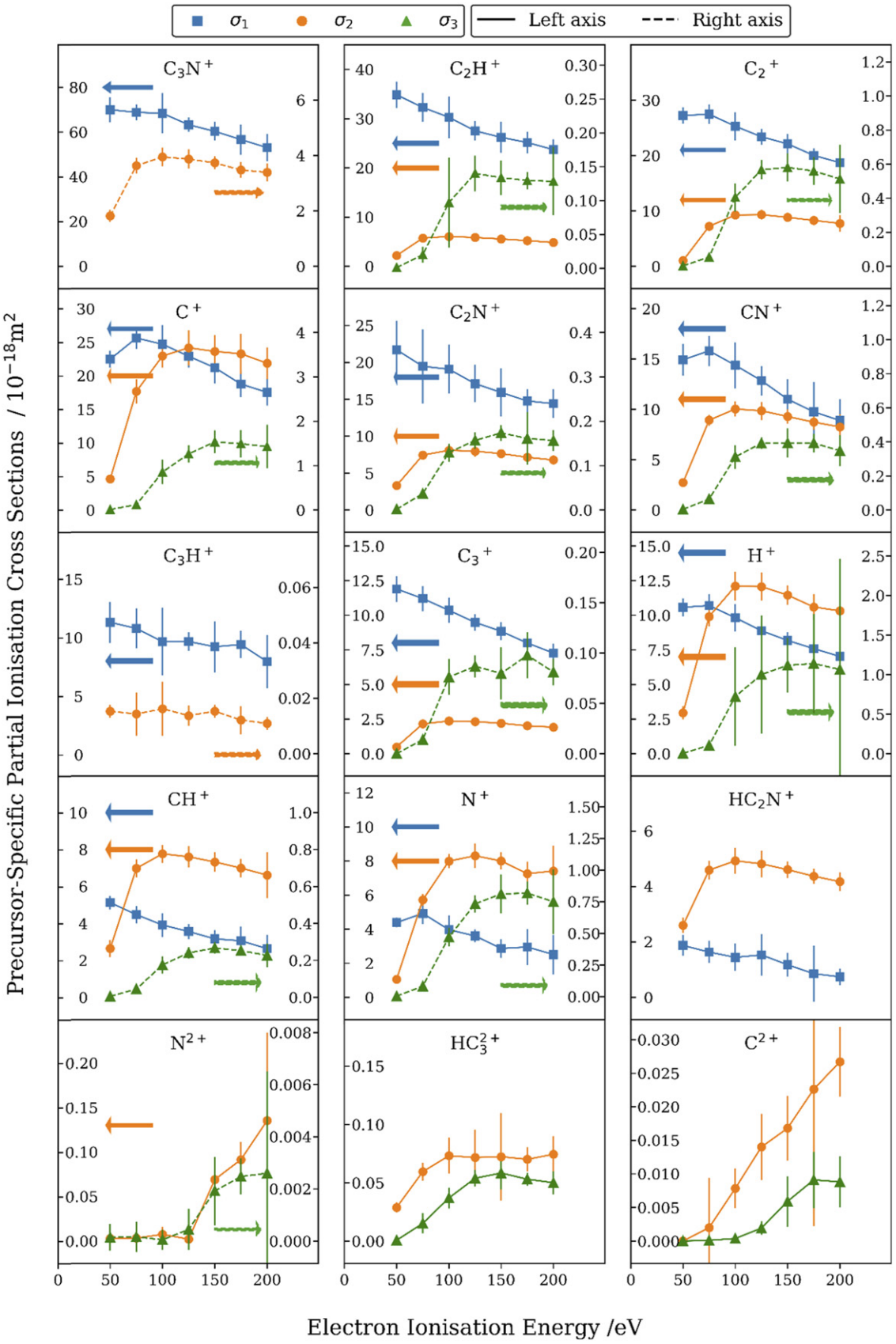

Figure 6. Precursor-specific partial electron ionisation cross sections for various fragment ions following electron ionisation of HC_3N. These cross sections quantify the contribution of single (σ_1), double (σ_2), and triple (σ_3) ionisation to the yield of each ion. Note the scale differences to earlier figures representing the PICS.

Table 1. Results of electronic structure calculations investigating the cyanoacetylene neutral, cation, and dication. A large number of bound dication geometries were discovered and only a pertinent subset are listed below. The full results of the computational investigations can be found in the supplementary information (tables S3–S5). A B3LYP algorithm with cc-VTZ basis set was employed, see text for details. Energies are expressed relative to the ground state of the neutral HCCCN molecule. AIE = adiabatic ionisation energy (zero point energy corrected); VIE = vertical ionisation energy.

Structure name	Geometry	Multiplicity	Charge	AIE (eV)	VIE (eV)
HCCCN neutral	Linear	1	0	—	—
2HCCCN+ cation	Linear	2	1	11.5	11.7
1HCCCN++ dication	Linear	1	2	30.3	30.6
3HCCCN++ dication	Linear	3	2	30.1	30.2
Bent 1C-CCNH++ dication	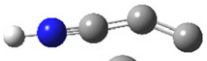	1	2	30.5	—
Diamond cyclic 1cycCCCNH++ dication	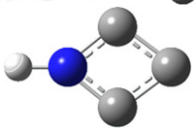	1	2	32.5	—

and cation geometry [19], and the associated ionisation energy [19], reported in the literature are in good accord with our calculations, validating our methodology given the accuracy of the dication energetics we extract from our experiments. For example, the reported first ionisation energy of HCCCN of 11.6 eV [19] is within 0.1 eV of the vertical ionisation energy that we determine. The dication (HC_3N^{2+}) appearance energy has been previously determined in 1986 from experimental work to be 31.52 ± 0.15 eV [16], slightly higher than the linear dication vertical ionisation potential of 30.2 eV of our computational work (see table 1). The computational investigation revealed that the geometric landscape of $[HC_3N]^{2+}$ is rich, with a number of local minima. Several cyclic geometries of the dication were discovered, examples of which are shown in table 1, with more details given in the supplementary information. These unusual minima, with connectivity markedly different to that of the neutral molecule, may explain our observation of fragment ions with unexpected connectivity, such as HC_2N^+.

To support the above argument, we have investigated if any of these cyclic minima could be accessed at our ionising energies, and thus account for some of the 'unusual' ions we observe in the pairs spectrum. To this end we performed a preliminary computational investigation of the energetics of the pathway between the bent 1C-CCNH++ dication geometry and the diamond-shaped singlet cyclic 1cycCCCNH++ geometry (table 1). A QST3 algorithm, using the B3LYP/cc-pVTZ methodology employed earlier, located a transition state connecting these minima (figure 7). The AIP of this transition state is 33.4 eV, a similar energy to the energies of many of the minima on the dicationic energy landscape. This observation hints that the barriers between the various dicationic minima on the $[HCCCN]^{2+}$ potential energy surface are relatively small, in comparison to the likely internal energy in the dication. Hence, we would expect a wide variety of dicationic geometries to be accessible upon double ionisation of HC_3N. This conclusion supports our explanation of the observation of a number of fragment ions with a connectivity markedly different to that of the neutral molecule. That is such ions can result from facile rearrangement of the dication. Such fluxionality of dicationic structures has been characterized before for a number of molecules [56, 57].

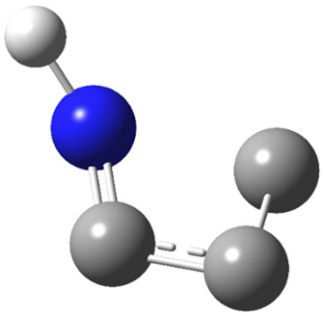

Figure 7. Transition state connecting the 1C-CCNH++ singlet geometry and the 1cycCCCNH++ diamond cyclic singlet geometry. See text for details.

3.3. Charge separating dissociation of $HCCCN^{2+}$

As described above, we can determine the KER for a given charge-separating dissociation of HC_3N^{2+} by fitting the time-of-flight difference ($t_1 - t_2$) spectra extracted from the experimental pairs data, for that dissociation, with a Monte-Carlo simulation. Several cation pairs from the pairs spectrum recorded following ionisation of HC_3N were chosen for such an analysis on the basis of clear, symmetric, and intense pair peaks. The KERs determined for these selected channels are shown in table 2. All KER determinations were made with data recorded at an ionising energy of 75 eV. This energy was chosen as the lowest ionising energy where the channels have sufficient intensity for robust analysis; the lowest possible ionisation energy restricts the number of accessible dication states and limits any contribution from triple ionisation. Several of the pairs channels show peak-shapes consistent with multiple dissociation pathways, with sloped/stepped rising and falling edges, as seen in figure 2(d). Conversely, a dissociation pathway with a single KER, has rather steeper rising and falling edges, as seen in figure 2(e). It is hard to see these subtle

Table 2. KER (T) and derived precursor dication state energy ($E[HC_3N^{2+}]$) determined for selected charge-separating processes of $[HCCCN]^{2+}$. Energies are expressed relative to the ground state of the neutral molecule. Some channels require two KERs to achieve a satisfactory fit of the experimental data. Uncertainties in these values are of the order of ±0.5 eV. Neutral third fragments are assumed not to dissociate where present. See text for details.

Ion A	Ion B	T_1 (eV)	T_2 (eV)	Intensity KER1:KER2	$E[HC_3N^{2+}]$, KER1 (eV)	$E[HC_3N^{2+}]$ KER 2 (eV)
CN^+	C_2^+	3.4			40.2	
C^+	N^+	3.1	5.1	0.4:0.6	44.0	46.0
C_2^+	C^+	3.5	6	0.35:0.65	42.6	45.1
C_2H^+	C^+	3.7	6.1	0.35:0.65	41.7	44.1
CN^+	C^+	4.9	7.5	0.5:0.5	44.3	46.9
C_2^+	CH^+	3.8			42.0	
CN^+	CH^+	5.4			44.1	
C_2^+	N^+	3.2	5.9	0.35:0.65	45.3	48.0
C_2H^+	N^+	5.4			46.6	
C_2N^+	C^+	3.8			39.0	
C_2N^+	CH^+	3.6			34.7	
C_3^+	N^+	4.4	2.9	0.5:0.5	42.1	40.6
C_3H^+	N^+	3.5			35.9	

Table 3. Dissociation pathways of cyanoacetylene assigned via momentum analysis. See text for details. The first five rows report the two-body dissociations we detect.

Ion pair	Proposed initial charge separation	Expected peak slope	Measured peak slope
$C_3H^+ + N^+$		−1	−1
$C_2N^+ + CH^+$		−1	−1
$HC_2N^+ + C^+$		−1	−1
$C_2H^+ + CN^+$		−1	−1
$C_3N^+ + H^+$		−1	−1
$C^+ + N^+$	$HCCC^+ + N^+$	−0.32	−0.4
$C_2^+ + N^+$	$HCCC^+ + N^+$	−1.54	−1.4
$C_3^+ + N^+$	$HCCC^+ + N^+$	−1.02	−1.1
$CN^+ + CH^+$	$HCC^+ + CN^+$	−0.48	−0.9
$CN^+ + C_2^+$	$HCC^+ + CN^+$	−0.96	−0.9
$CN^+ + C^+$	$HCC^+ + CN^+$	−0.48	−0.6
$C_2H^+ + C^+$	$HCC^+ + CN^+$	−0.46	−0.5
$C_2N^+ + C^+$	$HC^+ + CCN^+$	−0.92	−0.9
$C_2^+ + CH^+$	$HC^+ + CCN^+$	−1.58	−2.0
$C_2^+ + C^+$	$HCC^+ + CN^+$	−0.48	−0.65

changes in the 2D (pairs) coincidence spectrum figure 2(c). Hence the $t_1 - t_2$ spectra are required to reveal these subtleties of the KER distributions. For those coincidence peaks that require more than one KER for a satisfactory fit, two KERs have been employed to achieve a fit (table 2). A clear interpretation of such multiple KERs in a given dissociation channel is that more than one dicationic state contributes to the formation of the associated cation pair. The ratio of the two KERs in a given simulation is reported in table 2. As discussed above, the KERs are then used together with relevant thermodynamic data to define a lower bound for the energy of the dication state (the precursor state energy) from which the dissociation originated (equation (10)). The thermodynamic data required to determine these precursor state energies are all available in the literature [16, 58–68]. It is notable (table 2) that the energies of the dication states we determine all range between about 6 and 16 eV above the lowest calculated double ionisation energy (table 1). In our previous investigations [23, 34], precursor state energies determined in the above manner usually agreed well with calculated energies of the lower energy states of the associated dication. Hence, for cyanoacetylene, the fact that the charge-separating dissociation reactions appear to originate from states at energies markedly above the lowest lying dication states indicates that the low-lying states of $HCCCN^{2+}$ are predominantly long-lived and do not readily dissociate. Indeed, as many of the coincidence cation pairs we observe require considerable fragmentation of a strongly bonded dication, it is not unexpected that high energies are required to fragment such a species. Such a conclusion is supported by the low PS-PICS we report for dissociative double ionisation at 50 eV, where population of these long-lived dication states will dominate. We hope these observations prompt a more detailed computational investigation of the potential energy surfaces of the low lying states of $HCCCN^{2+}$.

As has been discussed extensively in the literature, the ‘shape’ of the pairs peak, for a given dicationic charge-separating reaction, in the pairs spectrum can reveal details of

the dynamics of the decay process [34, 41]. For example, the 'slope' of the coincidence peak in the pairs spectrum reveals the ratio of the momenta of the monocations involved [41]. Two extremes of peak slope are highlighted on the 2D coincidence mass spectrum in figure 2(b), and it is clear that the peak slopes vary for several other peaks in this region of the pairs spectrum. To this end, the form of the coincidence signals for several of the three-body dissociations we detect were further investigated in order to probe their dissociation pathways. As in previous work using this apparatus, the temporal width of our ionizing electron pulse restricts the detail we can extract from the peak shape, in comparison with more temporally resolved investigations [38]. However, we can compare the measured 'slope' of the coincidence peak with the value predicted by a proposed slow sequential decay from an initial dicationic two-body charge separation. For example, the formation of A^+ and C^+ from ABC^{2+} can proceed via one of the two pathways illustrated in equations (11) and (12), if we restrict ourselves to slow sequential decays. We can determine, via momentum analysis, the expected peak slopes for these two prospective decay channels and if one agrees well with experiment, we have good evidence to assign the decay pathway. Clearly if the possible pathways result in similar predicted slopes, a definitive mechanistic conclusion is not possible. If the experimental slope differs markedly from all the predictions for slow sequential decays, clearly an alternative mechanism is operating. This comparative approach has proved successful in probing the dissociation pathways of a number of dications, giving results in agreement with other groups [69, 70].

$$ABC^{2+} \rightarrow AB^+ + C^+ \qquad AB^+ \rightarrow A^+ + B \tag{11}$$

$$ABC^{2+} \rightarrow A^+ + BC^+ \qquad BC^+ \rightarrow B + C^+. \tag{12}$$

Table 3 shows the calculated peak slopes for a proposed dissociation pathway, and a comparison with the experimental value, for a number of the observed three-body charge-separating dissociation reactions of $HCCCN^{2+}$. The experimental peak slopes have an uncertainty of approximately 0.1, this value is determined by the coincidence statistics. Table 3 shows we obtain a very encouraging agreement between predicted and observed peak slopes, for a series of slow sequential decay mechanisms based on the fragmentation of the nascent ions generated in the two-body charge-separation reactions we observe experimentally. Observed peak slopes lying slightly closer to -1 than the calculated slope are indicative of the decay of the nascent monocation occurring when the Coulomb fields from the primary fragments can interact significantly, a fast sequential decay. As table 3 shows, this good agreement exists for all ion pairs except for $CN^+ + CH^+$ and $CC^+ + CH^+$. For the $CN^+ + CH^+$ channel, the measured peak slope lies well away from the predicted slope and much closer to -1, an indication that this reaction is very 'fast' and perhaps almost an instantaneous explosion. In the case of $CC^+ + CH^+$, the measured slope (-2.0) is more negative than the calculated slope (-1.58) for a slow sequential decay. The manner of this deviation points to a significant energy release in the decay of the nascent monocation, where the impulse to the heavier fragment (CC^+) is in the opposite direction to that from the initial charge separating step. Notably, while the two-body fragmentation to form $HCCN^+ + C^+$ is seen in the spectrum, none of the investigated three-body reactions appear to arise from this initial charge separation. This observation may indicate that the alternative geometries of $[HCCCN^{2+}]$ discussed above do not contribute significantly to the dissociation reactions we probe in table 3.

4. Conclusion

This study provides new information on the electron ionisation and subsequent dissociation of the astrochemically relevant species cyanoacetylene. Coincidence mass spectra involving the electron ionisation of cyanoacetylene in the gas phase have been recorded over the electron energy range 50 eV to 200 eV. From this experimental data, relative PICSs, and relative PS-PICSs have been determined. A BEB calculation of the total electron ionisation cross section of cyanoacetylene is then used to place these experimental results on an absolute scale, providing the first absolute PICSs data for this molecule. The parent cation dominates the mass spectrum, and the parent dication, HC_3N^{2+}, has a yield comparable with many of the fragment cations formed by single ionisation events. Two ions are detected which indicate there is an opportunity for marked structural rearrangement before the dissociation of both the monocation and dication: HCN^+ and HC_2N^+. A computational investigation hints at a rich dicationic energy landscape, in both the lowest energy singlet and triplet states. Specifically, several cyclic and bent geometries of the cyanoacetylene dication were located, as well as geometries involving H migration to the N atom, for both singlet and triplet multiplicities. Analysis of the kinetic energy releases accompanying the ion pairs that result from fragmentation of the dication indicate the dicationic states responsible for these fragmentations lie 6 to 16 eV above the vertical ionisation energy we calculate for the linear ground state singlet dication (30.6 eV). The fragment cation pairs we observe stem from three fundamental charge separating processes.

Acknowledgments

SDP and LE-G thank the Leverhulme Trust (RPG-2017-309) the EPSRC (EP/J010839/1), the Royal Society of Chemistry (E21-4679591105) and UCL for funding the work in the Chemistry Department. BC thanks STFC for funding her fellowship ST/R005133/1 'integrated software for electron-molecule collisions'. We thank Dr D Whitaker and Professor M Powner of UCL Chemistry for providing the cyanoacetylene sample.

Data availability statement

The data that support the findings of this study are available upon reasonable request from the authors.

ORCID iDs

Lilian K Ellis-Gibbings https://orcid.org/0000-0003-3083-157X
Bridgette Cooper https://orcid.org/0000-0002-4679-3240
Jonathan Tennyson https://orcid.org/0000-0002-4994-5238
Stephen D Price https://orcid.org/0000-0001-9007-2101

References

[1] Turner B E 1971 *Astrophys. J.* **163** L35
[2] Kunde V G, Aikin A C, Hanel R A, Jennings D E, Maguire W C and Samuelson R E 1981 *Nature* **292** 686
[3] Arumainayagam C R *et al* 2019 *Chem. Soc. Rev.* **48** 2293
[4] Hänni N, Altwegg K, Balsiger H, Combi M, Fuselier S A, De Keyser J, Pestoni B, Rubin M and Wampfler S F 2021 *Astron. Astrophys.* **647** A22
[5] Anderson C M, Samuelson R E, Bjoraker G L and Achterberg R K 2010 *Icarus* **207** 914
[6] Huang L C L, Asvany O, Chang A H H, Balucani N, Lin S H, Lee Y T, Kaiser R I and Osamura Y 2000 *J. Chem. Phys.* **113** 8656
[7] Fukuzawa K and Osamura Y 1997 *Astrophys. J.* **489** 113
[8] Osamura Y, Fukuzawa K, Terzieva R and Herbst E 1999 *Astrophys. J.* **519** 697
[9] Snow T P, Stepanovic M, Betts N B, Eichelberger B R, Martinez O Jr and Bierbaum V M 2009 *Astrobiology* **9** 1001
[10] Larsson M, Geppert W D and Nyman G 2012 *Rep. Prog. Phys.* **75** 066901
[11] Stairs S, Nikmal A, Bar D K, Zheng S L, Szostak J W and Powner M W 2017 *Nat. Commun.* **8** 15270
[12] Cordiner M A, Nixon C A, Charnley S B, Teanby N A, Molter E M, Kisiel Z and Vuitton V 2018 *Astrophys. J.* **859** L15
[13] Milburn R K, Hopkinson A C, Sun J, Bohme D K, Milburn R K, Hopkinson A C, Sun J and Bohme D K 1999 *J. Phys. Chem. A* **103** 7528
[14] Kaur J, Mason N and Antony B 2016 *J. Phys. B: At. Mol. Opt. Phys.* **49** 225202
[15] Gilmore T and Field T 2015 *J. Phys. B: At. Mol. Opt. Phys.* **48** 035201
[16] Harland P W 1986 *Int. J. Mass Spectrom. Ion Process.* **70** 231
[17] Leach S, Garcia G A, Mahjoub A, Bénilan Y, Fray N, Gazeau M-C, Gaie-Levrel F, Champion N and Schwell M 2014 *J. Chem. Phys.* **140** 174305
[18] Botschwina P, Horn M, Seeger S and Flügge J 1993 *Mol. Phys.* **78** 191
[19] Desrier A, Romanzin C, Lamarre N, Alcaraz C, Gans B, Gauyacq D, Liévin J and Boyé-Péronne S 2016 *J. Chem. Phys.* **145** 234310
[20] Dibeler V H, Reese R M and Franklin J L 1961 *J. Am. Chem. Soc.* **83** 1813
[21] Vieira Mendes L A, Boyé-Péronne S, Jacovella U, Liévin J and Gauyacq D 2012 *Mol. Phys.* **110** 2829
[22] Douglas K M and Price S D 2011 *Int. J. Mass Spectrom.* **303** 147
[23] Ellis-Gibbings L K, Fortune W G, Cooper B, Tennyson J and Price S D 2021 *Phys. Chem. Chem. Phys.* **23** 11424
[24] Love N A and Price S D 2004 *Phys. Chem. Chem. Phys.* **6** 4558
[25] Wiley W C and McLaren I H 1955 *Rev. Sci. Instrum.* **26** 1150
[26] Calandra P, O'Connor C S S and Price S D 2000 *J. Chem. Phys.* **112** 10821
[27] Bruce M R and Bonham R A 1992 *Z. Phys.* D **24** 149
[28] Bruce M R and Bonham R A 1993 *Int. J. Mass Spectrom. Ion Process.* **123** 97
[29] Bruce M R, Mi L, Sporleder C R and Bonham R A 1994 *J. Phys. B: At. Mol. Opt. Phys.* **27** 5773
[30] Dannhauser W and Flueckinger A F 1963 *J. Chem. Phys.* **38** 69
[31] Weast R C and Grasselli J G (ed) 1989 *CRC Handbook of Data on Organic Compounds* 2nd edn (Boca Raton, FL: CRC Press)
[32] Fletcher J D, Parkes M A and Price S D 2013 *J. Chem. Phys.* **138** 184309
[33] King S J and Price S D 2008 *Int. J. Mass Spectrom.* **277** 84
[34] King S J and Price S D 2007 *J. Chem. Phys.* **127** 174307
[35] King S J and Price S D 2008 *Int. J. Mass Spectrom.* **272** 154
[36] Straub H C, Renault P, Lindsay B G, Smith K A and Stebbings R F 1996 *Phys. Rev.* A **54** 2146
[37] McConkey J W, Malone C P, Johnson P V, Winstead C, McKoy V and Kanik I 2008 *Phys. Rep.* **466** 1
[38] Parkes M A, Douglas K M and Price S D 2019 *Int. J. Mass Spectrom.* **438** 97
[39] Harper S, Calandra P and Price S D 2001 *Phys. Chem. Chem. Phys.* **3** 741
[40] King S J 2008 *Studies of the Dissociation and Energetics of Gaseous Ions* (London: UCL Press)
[41] Eland J H D 1991 *Laser Chem.* **11** 259
[42] Thissen R, Delwiche J, Robbe J M, Duflot D, Flament J P and Eland J H D 1993 *J. Chem. Phys.* **99** 6590
[43] King S J and Price S D 2007 *J. Chem. Phys.* **127** 0
[44] Frisch M J *et al* 2016 *Gaussian 16, Revision A03*
[45] Kim Y-K and Rudd M E 1994 *Phys. Rev.* A **50** 3954
[46] Cooper B *et al* 2019 *Atoms* **7** 97
[47] Graves V, Cooper B and Tennyson J 2021 *J. Chem. Phys.* **154** 114104
[48] Lindsay B G, Rejoub R and Stebbings R F 2003 *J. Chem. Phys.* **118** 5894
[49] Rejoub R, Lindsay B G and Stebbings R F 2001 *J. Chem. Phys.* **115** 5053
[50] Wallace William E Cyanoacetylene 2021 *NIST Mass Spectral Library 1A V20* (Gaithersburg: National Institute of Standards and Technology)
[51] Cartwright D C *et al* 1984 *Electron–Molecule Interactions and Their Applications* (San Diego: Harcourt Brace Jovanovich)
[52] Linnartz H, Ioppolo S and Fedoseev G 2015 *Int. Rev. Phys. Chem.* **34** 205
[53] Armenta Butt S and Price S D 2020 *Phys. Chem. Chem. Phys.* **22** 8391
[54] Armenta Butt S and Price S D 2021 *Phys. Chem. Chem. Phys.* **23** 11287
[55] Price S D, Fletcher J D, Gossan F E and Parkes M A 2017 *Int. Rev. Phys. Chem.* **36** 145
[56] Roithová J and Schröder D 2007 *Phys. Chem. Chem. Phys.* **9** 2341
[57] Roithová J, Schwarz H and Schröder D 2009 *Chem. Eur. J.* **15** 9995–9
[58] Chase M W Jr 1992 *NIST-JANAF Thermochemical Tables* (*Journal of Physical and Chemical Reference Data Monograph* vol 9) 4th edn (Woodbury: American Institute of Physics)
[59] Tosi P, Lu W, Correale R and Bassi D 1999 *Chem. Phys. Lett.* **310** 180
[60] Melton C E 1966 *J. Chem. Phys.* **45** 4414
[61] Scheer M, Bilodeau R C, Brodie C a and Haugen H K 1998 *Phys. Rev.* A **58** 2844
[62] Reid C J, Ballantine J A, Andrews S R and Harris F M 1995 *Chem. Phys.* **190** 113

[63] Norwood K and Ng C Y 1989 *J. Chem. Phys.* **91** 2898
[64] Linstrom P J and Mallard W G (ed) *NIST Chemistry WebBook, NIST Standard Reference Database Number 69* (Gaithersburg: National Institute of Standards and Technology) (retrieved April 2021) p 20899
[65] Huber K P and Herzberg G 1979 *Molecular Spectra and Molecular Structure: IV. Constants of Diatomic Molecules* (New York: Springer)
[66] Lias S G, Bartmess J E, Liebman J F, Holmes J L, Levin R D and Mallard W G 1988 *J. Phys. Chem. Ref. Data* **17** 1
[67] Gupta S K and Gingerich K A 1979 *J. Chem. Phys.* **71** 3072
[68] Lide D R (ed) 1992 *Handbook of Chemistry and Physics* (Boca Raton, FL: CRC Press) pp 10–211
[69] Price S D 1992 *J. Phys. B: At. Mol. Opt. Phys.* **25** 3631
[70] Ward M D, King S J and Price S D 2011 *J. Chem. Phys.* **134** 024308